Environ Monit Assess (2020) 192:3
https://doi.org/10.1007/s10661-019-7973-3

Assessment of steady-state seepage through dams with nonsymmetric boundary conditions: analytical approach

Hamed Reza Zarif Sanayei · Hamed Javdanian

Received: 3 May 2019 / Accepted: 13 November 2019

Abstract In this study, new analytical solutions were developed for 2D and 3D steady-state water seepage through dams with nonsymmetric boundary conditions. The nonsymmetric boundary conditions for the 2D cases were created with different unit step functions on a part and/or parts of the right boundary of dam plane. Six cases were investigated in 2D, where a constant hydraulic head is applied at the left boundary of the dam plane and rectangular, ramp, triangular, trapezoidal, tunnel, and piecewise rectangular distributions of hydraulic head are applied at the right boundary of the dam plane. Then, a 3D case with a constant hydraulic head at the upstream and a linearly distributed hydraulic head at the downstream of the dam was investigated. Subsequently, the performance of proposed analytical solutions was examined by comparison with numerical finite difference modeling. The results demonstrate reasonable accuracy of the developed equations. The developed analytical solutions can be utilized as a benchmark to verify numerical models with similar boundary conditions.

Keywords Dam · Seepage · Analytical approach · Nonsymmetric boundary condition · Partial differential equation

H. R. Zarif Sanayei · H. Javdanian (✉)
Department of Civil Engineering, Shahrekord University, Shahrekord, Iran
e-mail: javdanian@sku.ac.ir

Introduction

Water seepage through the dam body has a vital role in the dam stability analysis. Therefore, hydraulic head determination and subsequently seepage flow simulation are among the design requisites in these structures. Water seepage into earth dams is illustrated by unconfined aquifer equation, a nonlinear partial differential equation (PDE) with limited analytical solutions (Zarif Sanayei et al. 2015, 2019). However, the choice of steady-state flow and homogeneous isotropic soil for unconfined aquifer make it feasible to acquire analytical solutions through classical approaches.

Tan et al. (2017) studied the effect of spatial variability of hydraulic parameters on the seepage flow in earth dams (Javdanian et al. 2018 a, b: Javdanian and Pradhan 2019; Shakarami et al. 2019; Javdanian 2019; Nasiri et al. 2019). Seepage flow through dams have been investigated by many researchers through finite difference (e.g., Fu and Jin 2009; Rakhshandehroo and Pourtouiserkani 2013), boundary elements (e.g., Chen et al. 1994; Leontiev and Huacasi 2001), and mesh-free numerical (e.g., Navas et al. 2016; Zhang et al. 2017) methods. Li et al. (2017) analyzed the seepage in roller compacted concrete dam using the finite element method (FEM). Nourani et al. (2014) proposed an arrangement of tubes analog and multiple reservoirs to simulate seepage flow through embankment dam conducting laboratory studies. An efficient technique to capture the seepage face boundary condition in finite element modeling of seepage problems in porous media (Fusi et al. 2015) was proposed by Pedroso (2015). Yuan and

Zhong (2016) developed a quadrature element formulation for 3D analysis of unconfined seepage in earth dams. A three-dimensional (3D) numerical analysis for unconfined seepage problems in anisotropic and inhomogeneous domains was developed by Kazemzadeh-Parsi and Daneshmand (2013). Fukuchi (2016) used the interpolation finite difference method (FDM) for numerical modeling of steady-state seepage problems. They reported that the proposed method is effective in the flow net calculation under mixed Dirichlet and Neumann conditions.

Analytical solutions give a better insight in comparison to the numerical modeling (Kacimov and Obnosov 2012, 2019; Wei et al. 2018). Kacimov and Obnosov (2012) developed analytical solutions for 2D seepage in dam core with uniform hydraulic head. Rezk and Senoon (2012) presented an analytical solution to calculate seepage through earth dam with upstream blanket. Teloglou and Bansal (2012) presented analytical solutions of Boussinesq equation to predict flow rate of water in an unconfined aquifer under transient seepage. Liang and Zhang (2013) derived analytical solutions for the lateral discharge and water table in a heterogeneous unconfined aquifer with fluctuating river stage. Closed-form analytical solutions to capture the influence of sea level rising on the unconfined sloping island aquifers were developed by Chesnaux (2016). El Tani et al. (2019) developed analytical equations for water table drawdown. Some analytical methods were also proposed by Mohsenian et al. (2019) for two-dimensional modeling of groundwater flow.

Reviewing the available literature indicates that most of the studies in the field of water seepage have been performed on the problems with symmetric boundary conditions by numerical methods. The current research focuses on the analytical solutions of two- and three-dimensional steady-state water seepage through dams with nonsymmetric boundary conditions. The boundary conditions for 2D cases are created with different unit step functions on a part and/or parts of the right boundary of the dam plane. In 2D cases, a constant hydraulic head is applied at the left boundary and various hydraulic head distributions are applied at the right boundary of the dam plane. Then, a 3D case is investigated. Subsequently, the performances of developed analytical solutions are examined using numerical modeling.

Governing equations

The equation for water flow in unconfined aquifer is developed by combining continuity and Darcy's law as a momentum equation. The equation for Cartesian coordinate in the inhomogeneous anisotropic soil with Dupuit assumptions is (Serrano and Workman 1998; Fukuchi 2016):

$$\frac{\partial h}{\partial t} = \frac{1}{S_y}\frac{\partial}{\partial x}\left(K_x h \frac{\partial h}{\partial x}\right) + \frac{1}{S_y}\frac{\partial}{\partial y}\left(K_y h \frac{\partial h}{\partial y}\right) \tag{1}$$

where h (L) is the hydraulic head, S_y is the specific yield, t (T) is the time, and K_x and $K_y\left(\frac{L}{T}\right)$ are the hydraulic conductivity of soil in x and y directions, respectively.

For an unconfined aquifer with steady-state flow in the isotropic homogeneous soil, Eq. (1) is written as:

$$\frac{\partial^2 h^2}{\partial x^2} + \frac{\partial^2 h^2}{\partial y^2} = 0 \tag{2}$$

Analytical solutions of Eq. (2) would express spatial variability of the hydraulic head in the unconfined aquifer sample under the given boundary conditions. In this research, new two-dimensional (2D) analytical solutions are developed for Eq. (2) subjected to nonsymmetric boundary conditions.

Analytical solution for 2D water seepage

In order to obtain closed-form analytical solution for Eq. 2, some simplifications need to be employed. A schematic rectangular cube of a homogeneous dam with various boundary and initial conditions is considered (Fig. 1a). Then, closed-form analytical solutions are investigated for the 2D horizontal plane (Fig. 1b) with nonsymmetric hydraulic head condition on the boundaries. In particular, constant hydraulic head is often applied on the left boundary and various hydraulic head distributions are applied on the right boundary (Fig. 1a, b).

Hydraulic head distribution

Rectangular distribution

The case is applicable where the outlet of a dam passes through a rectangular conduit and discharges into a channel, which creates a constant head at a part of the downstream of the dam. A constant hydraulic head is applied at the left boundary and a rectangular distribution of

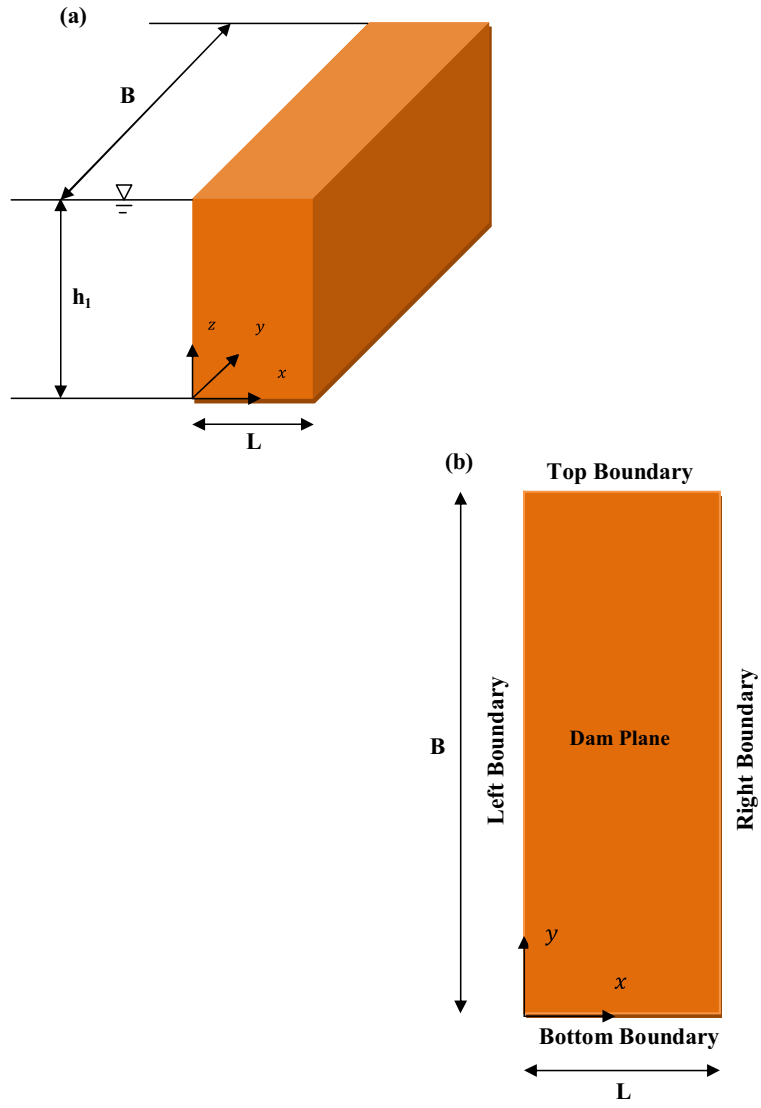

Fig. 1 **a** Schematic rectangular cube of a homogeneous dam. **b** 2D horizontal plane of the dam

hydraulic head is applied at the right boundary of the dam plane. In addition, the top and the bottom boundaries have no-flow boundary conditions (Fig. 1b). The boundary conditions for are expressed as:

$$h(0,y) = h_1 \qquad (3-\text{a})$$

$$h(L,y) = \frac{h_1}{a} * \left[U(y) - U\left(y - \frac{B}{10}\right) \right] \qquad (3-\text{b})$$

$$\frac{\partial h}{\partial y}(x,0) = 0 \quad \frac{\partial h}{\partial y}(x,B) = 0 \qquad (3-\text{c})$$

where U is the unit step function, and h_1 and a are constants.

A schematic view of the right boundary condition (Eq. 3-b) with $a = 3$, $h_1 = 300$ cm, and $B = 500$ cm is depicted in the Fig. 2. As depicted in this figure, the boundary condition presents the constant hydraulic head for all points at $0 \le y \le \frac{B}{10}$ and creates zero hydraulic head in other points. To find an analytical solution for Eq. (2) with the aforementioned boundary conditions, the variable change $h^2(x,y) = w(x,y)$ is used. Then, the partial differential equation (PDE) and the boundary conditions for $w(x,y)$ are written as:

$$\frac{\partial^2 w}{\partial x^2} + \frac{\partial^2 w}{\partial y^2} = 0 \qquad (4-\text{a})$$

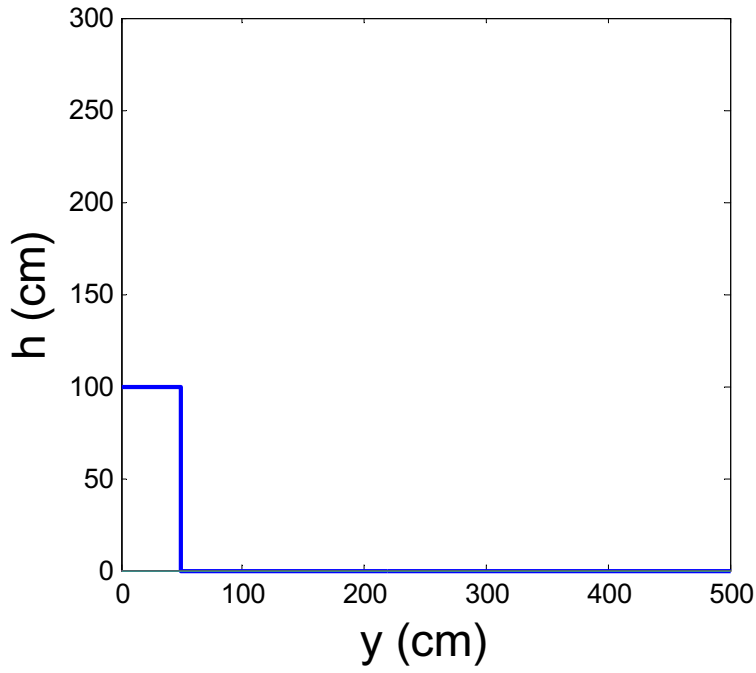

Fig. 2 Right boundary condition (Eq. 3-b) for the rectangular distribution case

$$w(0,y) = {h_1}^2 \qquad (4-\mathrm{b})$$

$$w(L,y) = \left(\frac{h_1}{a}\right)^2 * \left[U(y) - U\left(y - \frac{B}{10}\right)\right]^2 \qquad (4-\mathrm{c})$$

$$\frac{\partial w}{\partial y}(x,0) = 0 \qquad \frac{\partial w}{\partial y}(x,B) = 0 \qquad (4-\mathrm{d})$$

Using separation of variables for $w(x,y)$:

$$w(x,y) = X(x)\,Y(y) \qquad (5)$$

Then, substituting Eq. (5) into Eq. (4-a) and employing some simplifications gives:

$$\frac{Y''}{Y} = -\frac{X''}{X} = \mu \qquad (6)$$

where μ is an arbitrary constant.

If $\mu = 0$ and $\mu < 0$, assuming $\mu = -\lambda^2$ and $\lambda > 0$, then, $Y(y)$ in Eq. (6) has two answers considering the boundary conditions of Eq. (4-d), as follows:

$$Y_1 = B_1 \qquad (7)$$

$$Y_n = C_1 \cos(\lambda y) \quad , \qquad \lambda = \frac{n\pi}{B} \qquad n = 1,2,3,\ldots,\infty \qquad (8)$$

where B_1 and C_1 are constants.

Substituting $\mu = 0$ and $\mu = -\lambda^2$ in Eq. (6), two equations are obtained for $\frac{Y''}{Y}$ as follows:

$$-\frac{X''}{X} = 0 \qquad (9-\mathrm{a})$$

$$-\frac{X''}{X} = -\lambda^2 \qquad (9-\mathrm{b})$$

The solutions for Eqs. (9a) and (9b) are:

$$X_1 = C_2 x + C_3 \qquad (10-\mathrm{a})$$

$$X_n = C_4 \sinh(\lambda x) + C_5 \cosh(\lambda x) \qquad (10-\mathrm{b})$$

where C_2, C_3, C_4, and C_5 are constants.

By substituting Eq. (10-a) and Eq. (7) into Eq. (5), the first answer for $w(x,y)$ yields:

$$w_1(x,y) = X_1(x)Y_1(y) = C_2^* x + C_3^* \qquad (11)$$

where C_2^* is B_1C_2, and C_3^* is B_1C_3.

Also, by substituting Eq. (10-b) and Eq. (8) into Eq. (5), the second answer for $w(x,y)$ is written as:

$$w_2(x,y) = X_n(x)Y_n(y) = \sum_{n=1}^{\infty} \cos(\lambda y)\left[C_4^* \sinh(\lambda x) + C_5^* \cosh(\lambda x)\right] \quad (12)$$

where C_4^* is C_1C_4, and C_5^* is C_1C_5.

Finally, the overall answer for $w(x, y)$ is the combination of Eq. (11) and Eq. (12):

$$w(x,y) = w_1(x,y) + w_2(x,y) = C_2^* x + C_3^* + \sum_{n=1}^{\infty} \cos(\lambda y)\left[C_4^* \sinh(\lambda x) + C_5^* \cosh(\lambda x)\right] \quad (13)$$

By substituting the boundary conditions of Eq. (4-b) and Eq. (4-c) into Eq. (13) and using Fourier series properties for Eq. (13), the constant coefficients in Eq. (13) are written as:

$$C_2^* = \frac{1}{BL}\int_0^B \left(\frac{h_1}{a}\right)^2 \times \left[U(y) - U\left(y - \frac{B}{10}\right)\right]^2 dy - \frac{C_3^*}{L} = \frac{\frac{1}{10}\left(\frac{h_1}{a}\right)^2 - h_1^2}{L} \quad (14-a)$$

$$C_3^* = \frac{1}{B}\int_0^B h_1^2 dy = h_1^2 \quad (14-b)$$

$$C_4^* = \frac{\frac{2}{B}\int_0^B \left(\frac{h_1}{a}\right)^2 * \left[U(y) - U\left(y - \frac{B}{10}\right)\right]^2 \cos(\lambda y) dy - C_5^* \cosh(\lambda L)}{\sinh(\lambda L)} = \frac{2h_1^2 \sin\left(\frac{1}{10}n\pi\right)}{a^2 n\pi \sinh\left(\frac{n\pi L}{B}\right)} \quad (14-c)$$

$$C_5^* = \frac{2}{B}\int_0^B h_1^2 \cos(\lambda y) dy = 0 \quad (14-d)$$

Substituting Eq. (13) into $h^2(x, y) = w(x, y)$ gives:

$$h(x,y) = \sqrt{C_2^* x + C_3^* + \sum_{n=1}^{\infty} \cos(\lambda y)\left[C_4^* \sinh(\lambda x) + C_5^* \cosh(\lambda x)\right]} \quad (15)$$

Exact analytical solution of the problem (Eq. 15) satisfies the PDE (Eq. 2) and the boundary conditions (Eq. 3a–c). To confirm convergence of summations in Eq. (15), hydraulic head at different locations is computed using summations truncation with different amounts of n (Table 1). This table is presented for the parameters $a = 3$, $h_1 = 300$ cm, $L = 100$ cm, and $B = 500$ cm. As shown in Table 1, the change in the hydraulic head is negligible at different values of n. Also, the values are approximately equal at $n = 1$~15 and $n = 1$~20. To illustrate the application of the derived equations, hydraulic head values from an explicit scheme FDM solution (Eq. 2) is compared to the analytical solution (Eq. 15) for various amounts of x and y (Table 1, columns 7). Relative error (RE) (Javdanian and Lee 2019; Javdanian 2019) in Table 1 is calculated using Eq. (16):

$$RE = \frac{\left|h_{\text{analytical}} - h_{\text{numerical}}\right|}{\left|h_{\text{analytical}}\right|} \times 100\% \quad (16)$$

where, $h_{\text{analytical}}$ and $h_{\text{numerical}}$ are analytical-based and numerical-based hydraulic head, respectively.

As shown in Table 1, the values of RE are less than 3%. Figure 3 depicted hydraulic head contours calculated by Eq. (15). This figure shows the distribution of the hydraulic head that remains at $h = 300$ cm on the left ($x = 0$) and $h =$ Eq. (3-b) on the right boundaries ($x =$ 100 cm) of the dam plane. Hydraulic head contours are perpendicular to the top and bottom boundaries of the dam plane, confirming no-flow boundary condition.

Ramp distribution

Ramp distribution of the hydraulic head on the downstream of the dam body may be caused by the right triangular shape of the water outlet. In practice, this condition occurs during clogging of the sluice gate by sediments and debris. Mathematically, top and bottom, as well as the left boundary conditions, are as same as the rectangular distribution case. The right boundary is written as Eq. (17):

$$h(L,y) = \frac{h_1}{a} \times \frac{3}{B} \times \left(y - \frac{B}{3}\right) \times U\left(y - \frac{B}{3}\right) \times \left[U\left(y - \frac{B}{3}\right) - U\left(y - \frac{2B}{3}\right)\right] \quad (17)$$

The right boundary condition (Eq. 17) with $a = 3$, $h_1 = 300$ cm, and $B = 500$ cm was illustrated in Fig. 4. The boundary condition presents the ramp distribution of hydraulic head for $\frac{B}{3} \le y \le \frac{2B}{3}$. Following similar mathematical methods used for rectangular distribution case, the answer for $h(x, y)$ would be identical to Eq. (15) but with different coefficients. Mathematical forms of C_3^* and C_5^* are identical to the ones defined by Eq. (14); however, C_2^* and C_4^* are expressed as:

Table 1 Hydraulic head values resulted from analytical approach (for different summation truncations) and FDM for rectangular distribution case

x (cm)	y (cm)	$h_{analytical}$				h_{FDM}	RE (%)
		$n = 1\sim5$	$n = 1\sim10$	$n = 1\sim15$	$n = 1\sim20$	$\Delta x = 1$ cm and $\Delta y = 10$ cm	
60	100	203.12	203.26	203.34	203.34	198.45	2.40
50	50	228.47	228.63	228.81	228.81	223.36	2.38
70	300	175.65	175.89	176.15	176.15	172.41	2.12
40	300	242.06	242.21	242.35	242.35	238.62	1.53
80	80	148.12	148.33	148.48	148.48	145.13	2.25
80	250	144.38	144.52	144.65	144.65	141.51	2.17
90	50	128.54	128.73	128.91	128.90	125.26	2.82
90	350	102.17	102.39	102.66	102.66	99.92	2.66
20	150	273.37	273.58	273.81	273.81	270.03	1.38
10	400	286.81	287.03	287.29	287.29	285.30	0.69

$$C_2^* = \frac{1}{BL}\int_0^B \left(\frac{h_1}{a}\right)^2 \times \left(\frac{3}{B}\right)^2 \times \left[\left(y-\frac{B}{3}\right) \times U\left(y-\frac{B}{3}\right) \times \left[U\left(y-\frac{B}{3}\right) - U\left(y-\frac{2B}{3}\right)\right]\right]^2 dy - \frac{C_3^*}{L} = \frac{\frac{1}{9}\left(\frac{h_1}{a}\right)^2 - h_1^2}{L} \quad (18-a)$$

$$C_4^* = \frac{\frac{2}{B}\int_0^B \left(\frac{h_1}{a}\right)^2 \times \left(\frac{3}{B}\right)^2 \times \left[\left(y-\frac{B}{3}\right) \times U\left(y-\frac{B}{3}\right) \times \left[U\left(y-\frac{B}{3}\right) - U\left(y-\frac{2B}{3}\right)\right]\right]^2 \cos(\lambda y) dy}{\sinh(\lambda L)} = \frac{2h_1^2\left(18\sin\left(\frac{n\pi}{3}\right) + n^2\pi^2\sin\left(\frac{2n\pi}{3}\right) - 18\sin\left(\frac{2n\pi}{3}\right) + 6n\pi\cos\left(\frac{2n\pi}{3}\right)\right)}{a^2n^3\pi^3\sinh\left(\frac{n\pi L}{B}\right)} \quad (18-b)$$

where, λ is identical to the one defined for the rectangular distribution case.

Figure 5 shows the hydraulic head calculated by Eqs. (15) and (18) for $n = 1\sim20$. As seen in this figure, the ramp distribution of the hydraulic head on the right boundary of the dam plane creates a skewed shape in the hydraulic head contours. Figure 5 depicts distribution of the hydraulic head that remains at $h = 300$ cm on the left ($x = 0$) and $h =$ Eq. (17) on the right boundaries ($x = 100$ cm) of the dam plane.

Triangular distribution

Triangular distribution of the hydraulic head may be resulted by the equilateral triangular shape of the water outlet. In practice, this condition occurs

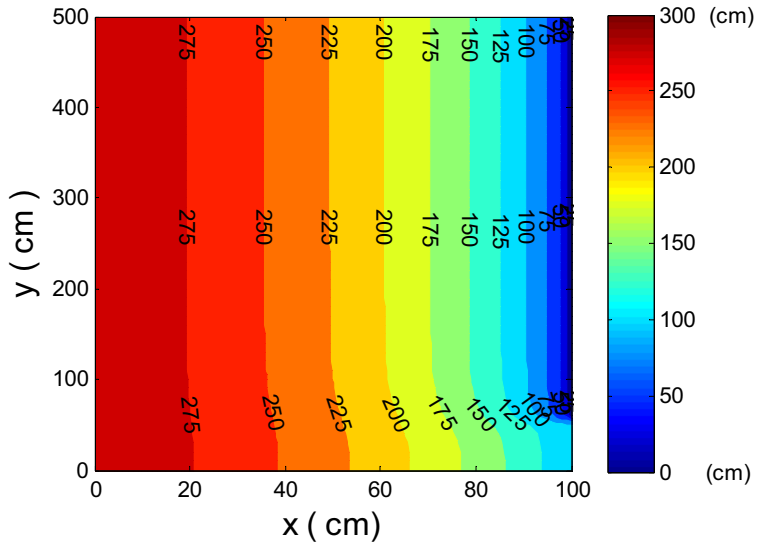

Fig. 3 Hydraulic head contours for the rectangular distribution case

during clogging of the sluice gate by sediments and debris. Mathematically, bottom and top boundary conditions as well as the left boundary condition are identical to rectangular distribution case. The right boundary is written as:

$$h(L,y)=\frac{h_1}{a}\times\left(U\left(y-\frac{B}{5}\right)\times\left(\frac{5}{B}*\left(y-\frac{B}{5}\right)\right)+U\left(y-\frac{2B}{5}\right)\times\left(-\frac{5}{B}\right)\times\left(\left(y-\frac{3B}{5}\right)+\left(y-\frac{B}{5}\right)\right)+U\left(y-\frac{3B}{5}\right)\left(\frac{5}{B}\times\left(y-\frac{3B}{5}\right)\right)\right) \tag{19}$$

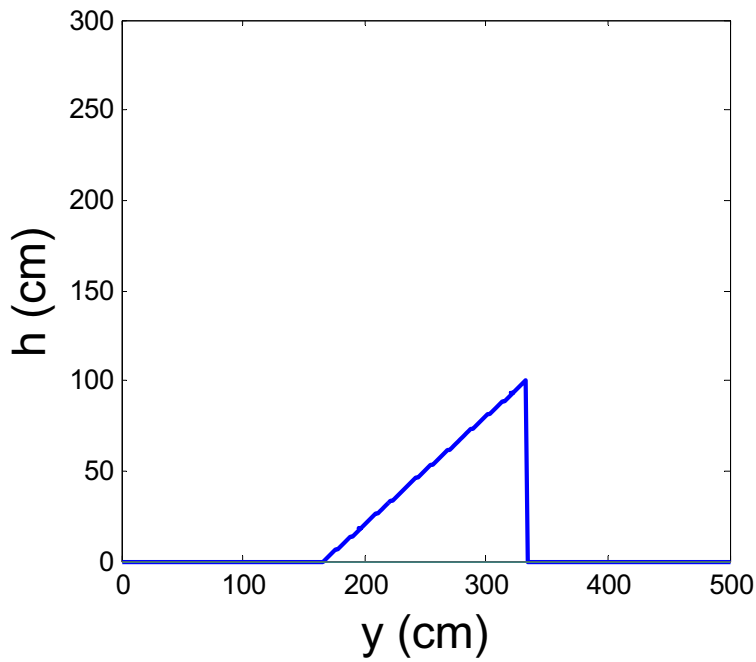

Fig. 4 Right boundary condition (Eq. 17) for the ramp distribution case

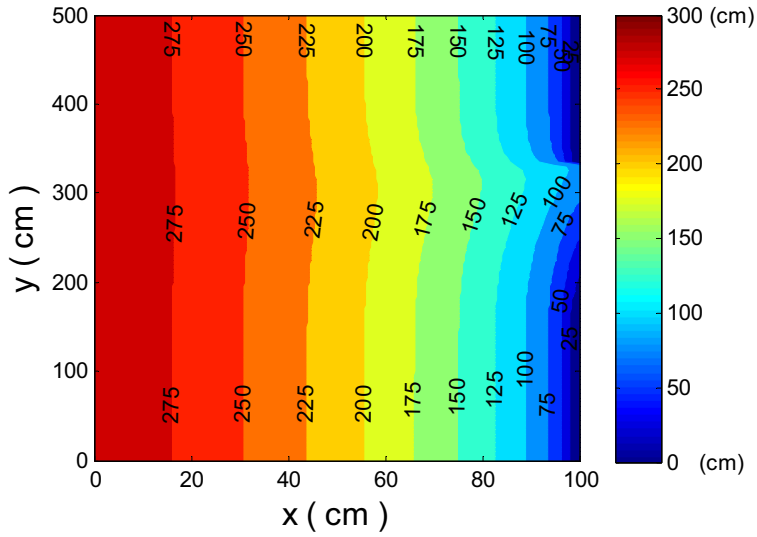

Fig. 5 Hydraulic head contours for the ramp distribution case

The right boundary condition (Eq. 19) with $a = 3$, $h_1 = 300$ cm, and $B = 500$ cm is shown in Fig. 6. As seen in Fig. 6, this boundary condition presents the triangular distribution of the hydraulic head for $\frac{B}{5} \le y \le \frac{3B}{5}$. The answer of $h(x, y)$ for triangular distribution case would be identical to Eq. (15) but with different coefficients. Mathematical forms of C_3^* and C_5^* are identical to Eq. (14); however, C_2^* and C_4^* are expressed as:

$$C_2^* = \frac{1}{BL}\int_0^B \left(\frac{h_1}{a}\right)^2 \times \left(U\left(y-\frac{B}{5}\right) \times \left(\frac{5}{B} * \left(y-\frac{B}{5}\right)\right) + U\left(y-\frac{2B}{5}\right) \times \left(-\frac{5}{B}\right) \times \left(\left(y-\frac{3B}{5}\right) + \left(y-\frac{B}{5}\right)\right) + U\left(y-\frac{3B}{5}\right)\left(\frac{5}{B} \times \left(y-\frac{3B}{5}\right)\right)\right)^2 dy - \frac{C_3^*}{L} = \frac{\frac{2}{15}\left(\frac{h_1}{a}\right)^2 - h_1^2}{L} \quad (20-\text{a})$$

$$C_4^* = \frac{\frac{2}{B}\int_0^B \left(\frac{h_1}{a}\right)^2 * \left(U\left(y-\frac{B}{5}\right) \times \left(\frac{5}{B} * \left(y-\frac{B}{5}\right)\right) + U\left(y-\frac{2B}{5}\right) \times \left(-\frac{5}{B}\right) \times \left(\left(y-\frac{3B}{5}\right) + \left(y-\frac{B}{5}\right)\right) + U\left(y-\frac{3B}{5}\right)\left(\frac{5}{B} \times \left(y-\frac{3B}{5}\right)\right)\right)^2 \cos(\lambda y) dy}{\sinh(\lambda L)} \quad (20-\text{b})$$

$$= \frac{2h_1^2\left(50\sin\left(\frac{n\pi}{5}\right) + 20n\pi\cos\left(\frac{2n\pi}{5}\right) - 50\sin\left(\frac{3n\pi}{5}\right)\right)}{a^2 n^3 \pi^3 \sinh\left(\frac{n\pi L}{B}\right)}$$

The hydraulic head (h) is calculated for $n = 1$~20 using Eqs. (15) and (20) and the contours was depicted in Fig. 7. As seen in this figure, the triangular distribution of the hydraulic head on the right boundary creates a tent shape in the hydraulic head contours.

Trapezoidal distribution

This case is applicable where the water outlet from the dam takes place through a trapezoidal gate valves. The right boundary is expressed as:

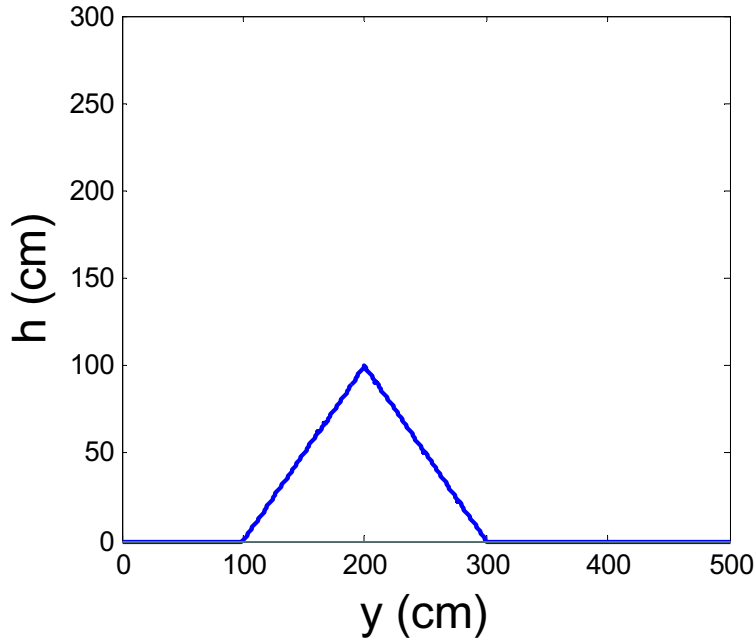

Fig. 6 Right boundary condition (Eq. 19) for the triangular distribution case

$$h(L,y) = \frac{h_1}{a} \times \left(U\left(y - \frac{B}{4}\right) \times \left(\frac{8}{B} \times \left(y - \frac{B}{4}\right)\right) + U\left(y - \frac{3B}{8}\right) \times \left(1 - \frac{8}{B}\left(y - \frac{B}{4}\right)\right) + U\left(y - \frac{5B}{8}\right)\left(-\frac{8}{B}\left(y - \frac{6B}{8}\right) - 1\right) + U\left(y - \frac{6B}{8}\right)\left(\frac{8}{B} \times \left(y - \frac{6B}{8}\right)\right)\right) \quad (21)$$

The right boundary condition of the trapezoidal distribution case (Eq. 21) with $a = 3$, $h_1 = 300$ cm, and $B = 500$ cm was shown in Fig. 8. As depicted in this figure, the boundary condition presents the trapezoidal distribution of the hydraulic head for $\frac{B}{4} \le y \le \frac{6B}{8}$. For the trapezoidal distribution case, the mathematical forms of C_3^* and C_5^* are identical to Eq. (14); however, C_2^* and C_4^* are expressed as:

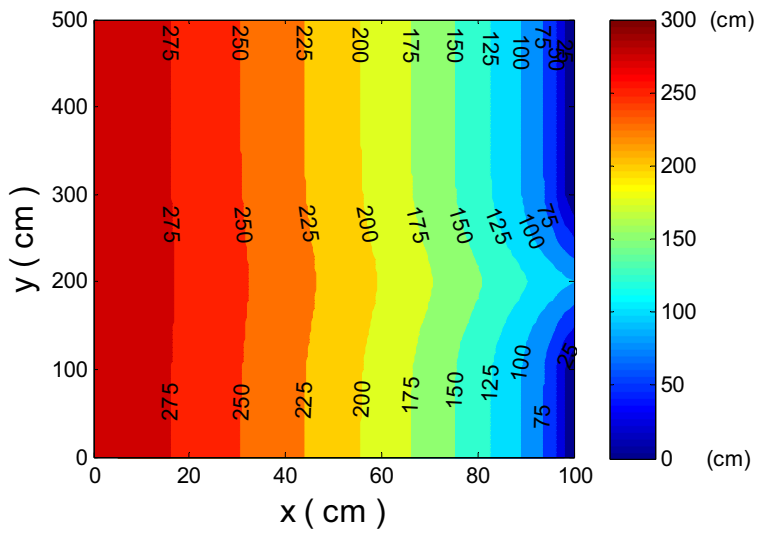

Fig. 7 Hydraulic head contours for the triangular distribution case

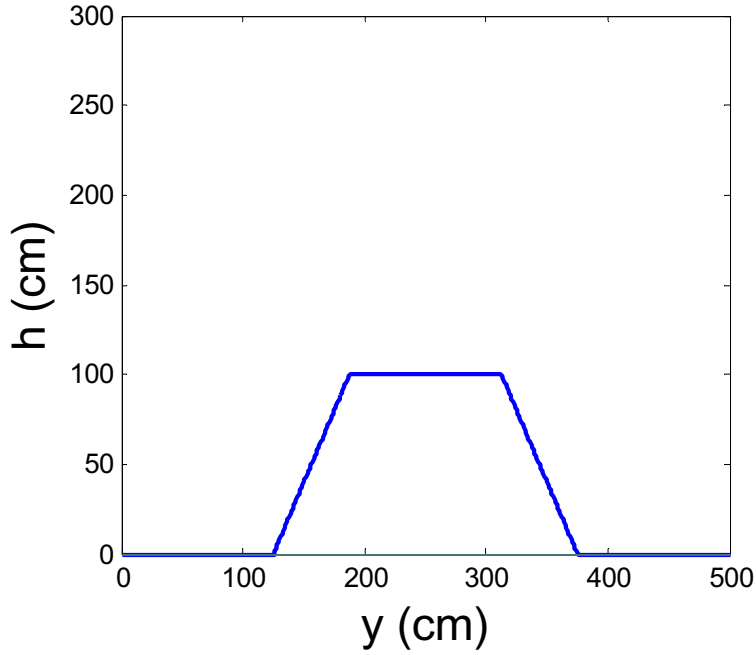

Fig. 8 Right boundary condition (Eq. 21) for the trapezoidal distribution case

$$C_2^* = \frac{1}{BL}\int_0^B \left(\frac{h_1}{a}\right)^2 \times \left(U\left(y-\frac{B}{4}\right)\times\left(\frac{8}{B}\times\left(y-\frac{B}{4}\right)\right)+U\left(y-\frac{3B}{8}\right)\times\left(1-\frac{8}{B}\left(y-\frac{B}{4}\right)\right)+U\left(y-\frac{5B}{8}\right)\left(-\frac{8}{B}\left(y-\frac{6B}{8}\right)-1\right)+U\left(y-\frac{6B}{8}\right)\left(\frac{8}{B}\times\left(y-\frac{6B}{8}\right)\right)\right)^2 dy - \frac{C_3^*}{L} = \frac{\frac{1}{3}\left(\frac{h_1}{a}\right)^2 - h_1^2}{L} \quad (22-a)$$

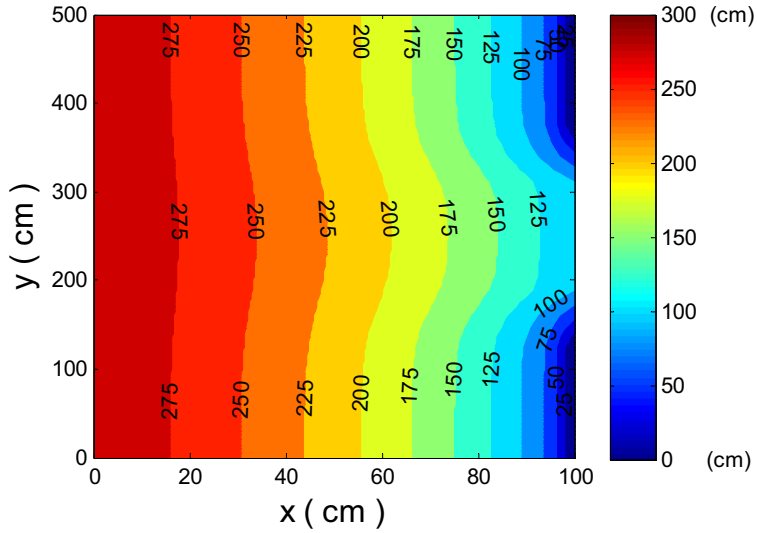

Fig. 9 Hydraulic head contours for the trapezoidal distribution case

$$C_4^* = \frac{\frac{2}{B}\int_0^B \left(\frac{h_1}{a}\right)^2 * \left(U\left(y-\frac{B}{4}\right)\times\left(\frac{8}{B}*\left(y-\frac{B}{4}\right)\right)+U\left(y-\frac{3B}{8}\right)\times\left(1-\frac{8}{B}\left(y-\frac{B}{4}\right)\right)+U\left(y-\frac{5B}{8}\right)\left(-\frac{8}{B}\left(y-\frac{6B}{8}\right)-1\right)+U\left(y-\frac{6B}{8}\right)\left(\frac{8}{B}\times\left(y-\frac{6B}{8}\right)\right)\right)^2\cos(\lambda y)dy}{\sinh(\lambda L)} \quad (22-b)$$

$$= \frac{2h_1^2\left(128\sin\left(\frac{n\pi}{4}\right)-128\sin\left(\frac{3n\pi}{8}\right)+128\sin\left(\frac{5n\pi}{8}\right)-128\sin\left(\frac{3n\pi}{4}\right)+16n\pi\cos\left(\frac{3n\pi}{8}\right)+16n\pi\cos\left(\frac{5n\pi}{8}\right)\right)}{a^2n^3\pi^3\sinh\left(\frac{n\pi L}{B}\right)}$$

Hydraulic head contours (Fig. 9) were calculated by Eqs. (15) and (22) for $n = 1\sim20$. As depicted in Fig. 9, the trapezoidal distribution of the hydraulic head on the right boundary creates a bend shape in the h contours

Tunnel distribution

In this case, the outlet conduit has a tunnel shape. Mathematically, the right boundary condition is rewritten as:

$$h(L,y) = \frac{h_1}{a}\times\left(U\left(y-\frac{B}{3}\right)\times\left(-\sin\left(\frac{\pi y}{B/3}\right)+1\right)+U\left(y-\frac{2B}{3}\right)\times\left(\sin\left(\frac{\pi y}{B/3}\right)-1\right)\right) \quad (23)$$

The right boundary condition (Eq. 23) with $a = 6$, $h_1 = 300$ cm, and $B = 500$ cm was shown in Fig. 10. This figure presents the tunnel distribution of the hydraulic head for $\frac{B}{3} \le y \le \frac{2B}{3}$. For the tunnel distribution case, mathematical forms of C_3^* and C_5^* are identical to Eq. (14) and C_2^* and C_4^* are expressed as:

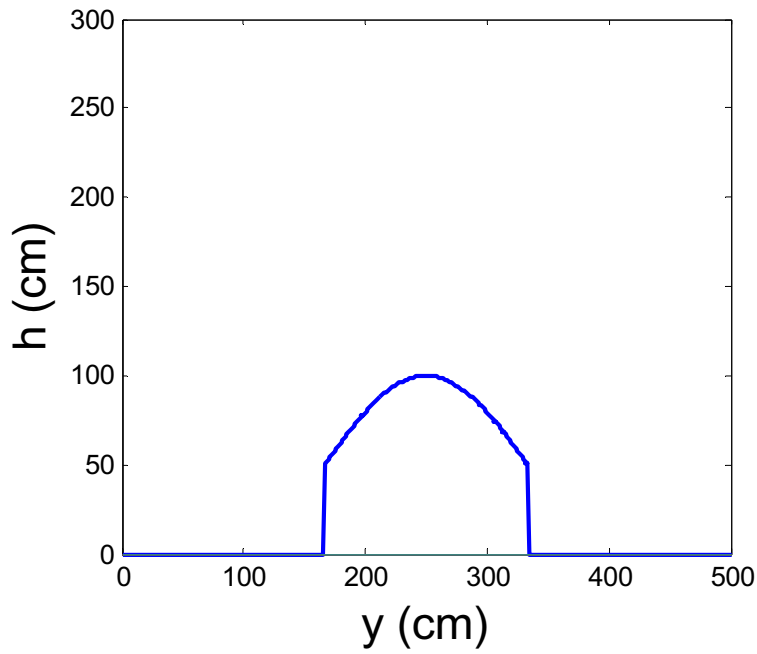

Fig. 10 Right boundary condition (Eq. 23) for the tunnel distribution case

$$C_2^* = \frac{1}{BL}\int_0^B \left(\frac{h_1}{a}\right)^2 \times \left(U\left(y-\frac{B}{3}\right) \times \left(-\sin\left(\frac{\pi y}{B/3}\right)+1\right) + U\left(y-\frac{2B}{3}\right) \times \left(\sin\left(\frac{\pi y}{B/3}\right)-1\right)\right)^2 dy - \frac{C_3^*}{L}$$
$$= \frac{\frac{1}{6}\frac{h_1^2(3\pi+8)}{a^2\pi} - h_1^2}{L} \qquad (24-a)$$

$$C_4^* = \frac{\frac{2}{B}\int_0^B \left(\frac{h_1}{a}\right)^2 * \left(U\left(y-\frac{B}{3}\right) \times \left(-\sin\left(\frac{\pi y}{B/3}\right)+1\right) + U\left(y-\frac{2B}{3}\right) \times \left(\sin\left(\frac{\pi y}{B/3}\right)-1\right)\right)^2 \cos(\lambda y)dy}{\sinh(\lambda L)} \qquad (24-b)$$
$$= \frac{-2h_1^2}{a^2 n\pi(n^4-45n^2+324)\sinh\left(\frac{n\pi L}{B}\right)} \times \left(486\sin\left(\frac{n\pi}{3}\right) - 486\sin\left(\frac{2n\pi}{3}\right) - n^4\sin\left(\frac{n\pi}{3}\right) - 63n^2\sin\left(\frac{n\pi}{3}\right) + 6n^3\cos\left(\frac{n\pi}{3}\right) - n^4\sin\left(\frac{2n\pi}{3}\right)\right.$$
$$\left. + 63n^2\sin\left(\frac{2n\pi}{3}\right) + 6n^3\cos\left(\frac{2n\pi}{3}\right) - 216n\cos\left(\frac{n\pi}{3}\right) - 216n\cos\left(\frac{2n\pi}{3}\right)\right)$$

In order to confirm convergence of summations in Eq. (15) with new coefficients, hydraulic head at different locations is calculated by summations truncation with different values of n (Table 2). The dam parameters utilized for the problem are similar to the rectangular distribution case. To illustrate the application of the derived equations, hydraulic head values from an explicit scheme FDM solution (Eq. 2) is compared to the analytical solution (Eq. 15) for different values of x and y (Table 2, columns 7). As presented in Table 2, the values of relative errors (*REs*) are less than 1%. Based on Eqs. (15) and (24), hydraulic head contours were

Table 2 Hydraulic head values resulted from analytical approach (for different summation truncations) and FDM for tunnel distribution case

x (*cm*)	y (*cm*)	$h_{analytical}$				h_{FDM}	*RE* (%)
		$n = 1\sim5$	$n = 1\sim10$	$n = 1\sim15$	$n = 1\sim20$	$\Delta x = 5$ cm and $\Delta y = 5$ cm	
95	250	105.57	115.93	115.68	115.60	116.69	0.94
90	250	128.64	131.27	131.52	131.57	132.70	0.85
80	250	156.21	157.91	157.72	157.78	158.92	0.72
70	250	179.42	180.53	180.72	180.78	181.56	0.43
60	250	201.17	201.28	201.49	201.57	202.64	0.53
20	250	270.24	270.39	270.39	270.39	270.87	0.17
90	100	90.12	95.11	94.95	95.08	95.24	0.16
80	350	137.24	135.61	135.65	135.68	135.83	0.11
70	400	163.25	164.57	164.60	164.61	164.86	0.15
30	400	250.99	251.17	251.17	251.17	251.31	0.05

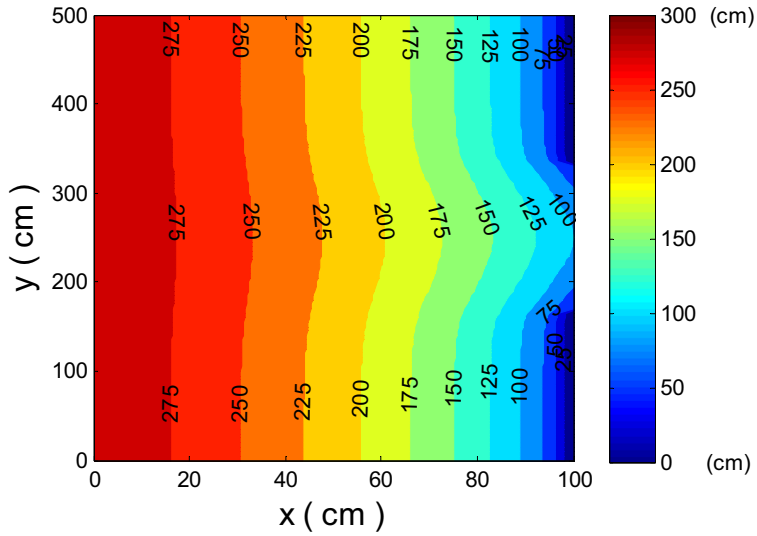

Fig. 11 Hydraulic head contours for the tunnel distribution case

depicted in Fig. 11. As seen in this figure, the tunnel distribution of the hydraulic head on the right boundary of the dam plane creates a bell shape contour. Figure 11 shows the distribution of the hydraulic head that remains at $h = 300$ cm on the left ($x = 0$) and $h =$ Eq. (23) on the right boundaries ($x = 100$ cm) of the dam plane.

Piecewise rectangular distribution

Piecewise rectangular distribution can also be justified similar to the trapezoidal and tunnel distributions cases where there are several rectangular outlets instead of a single outlet. The bottom, top, and left boundary conditions for the piecewise rectangular distribution case are identical to the previous cases. The mathematical form for the right boundary condition is written as:

$$h(L,y) = \frac{h_1}{a} \times \left(U(y) - U\left(y - \frac{B}{14}\right) + U\left(y - \frac{2B}{14}\right) - U\left(y - \frac{3B}{14}\right) + U\left(y - \frac{4B}{14}\right) - U\left(y - \frac{5B}{14}\right) + U\left(y - \frac{6B}{14}\right) \right) \quad (25)$$

The right boundary condition (Eq. 25) with $a = 3$, $h_1 = 300$ cm, and $B = 500$ cm was depicted in Fig. 12. As depicted in this figure, the boundary condition presents the constant hydraulic head for the ranges of $0 \le y \le \frac{B}{14}$, $\frac{2B}{14} \le y \le \frac{3B}{14}$, $\frac{4B}{14} \le y \le \frac{5B}{14}$ and $\frac{6B}{14} \le y \le \frac{7B}{14}$. The answer for $h(x, y)$ is similar to Eq. (15) but with different coefficients. Mathematical forms of coefficients C_3^* and C_5^* are identical to Eq. (14); however, coefficients C_2^* and C_4^* are expressed as:

$$C_2^* = \frac{1}{BL} \int_0^B \left(\frac{h_1}{a}\right)^2 \times \left(U(y) - U\left(y - \frac{B}{14}\right) + U\left(y - \frac{2B}{14}\right) - U\left(y - \frac{3B}{14}\right) + U\left(y - \frac{4B}{14}\right) - U\left(y - \frac{5B}{14}\right) + U\left(y - \frac{6B}{14}\right) \right)^2 dy - \frac{C_3^*}{L} = \frac{\frac{11}{14}\frac{h_1^2}{a^2} - h_1^2}{L} \quad (26 - a)$$

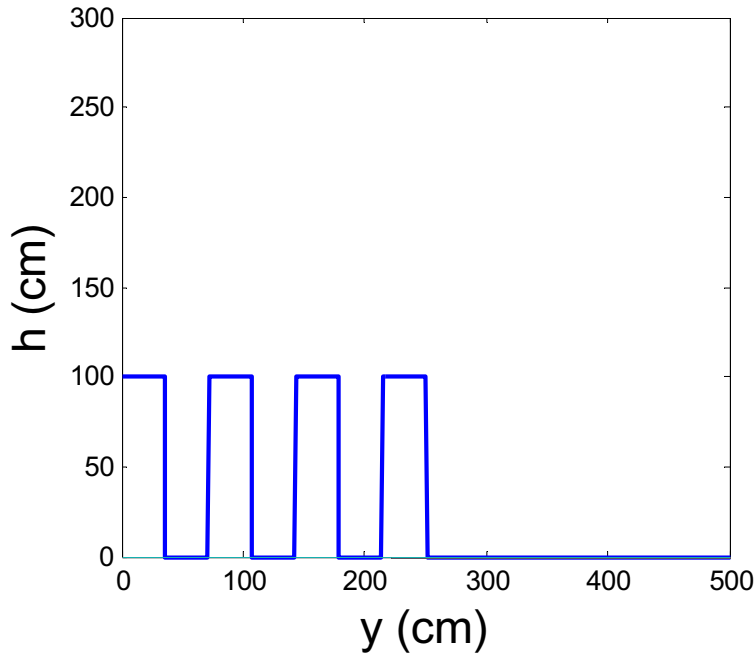

Fig. 12 Right boundary condition (Eq. 23) for the piecewise rectangular distribution case

$$C_4^* \qquad (26-\mathrm{b})$$

$$= \frac{\frac{2}{B}\int_0^B \left(\frac{h_1}{a}\right)^2 \times \left(U(y) - U\left(y-\frac{B}{14}\right) + U\left(y-\frac{2B}{14}\right) - U\left(y-\frac{3B}{14}\right) + U\left(y-\frac{4B}{14}\right) - U\left(y-\frac{5B}{14}\right) + U\left(y-\frac{6B}{14}\right)\right)^2 \cos(\lambda y)dy}{\sinh(\lambda L)}$$

$$= \frac{2h_1^2\left(\sin\left(\frac{n\pi}{14}\right) - \sin\left(\frac{n\pi}{7}\right) + \sin\left(\frac{3n\pi}{14}\right) - sin\left(\frac{2n\pi}{7}\right) + \sin\left(\frac{5n\pi}{14}\right) - sin\left(\frac{3n\pi}{7}\right)\right)}{a^2 n\pi \sinh\left(\frac{n\pi L}{B}\right)}$$

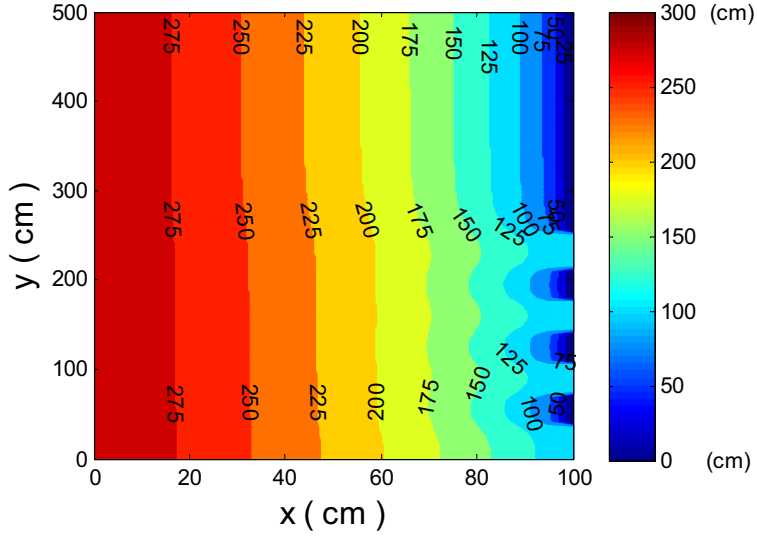

Fig. 13 Hydraulic head contours for the piecewise rectangular distribution case

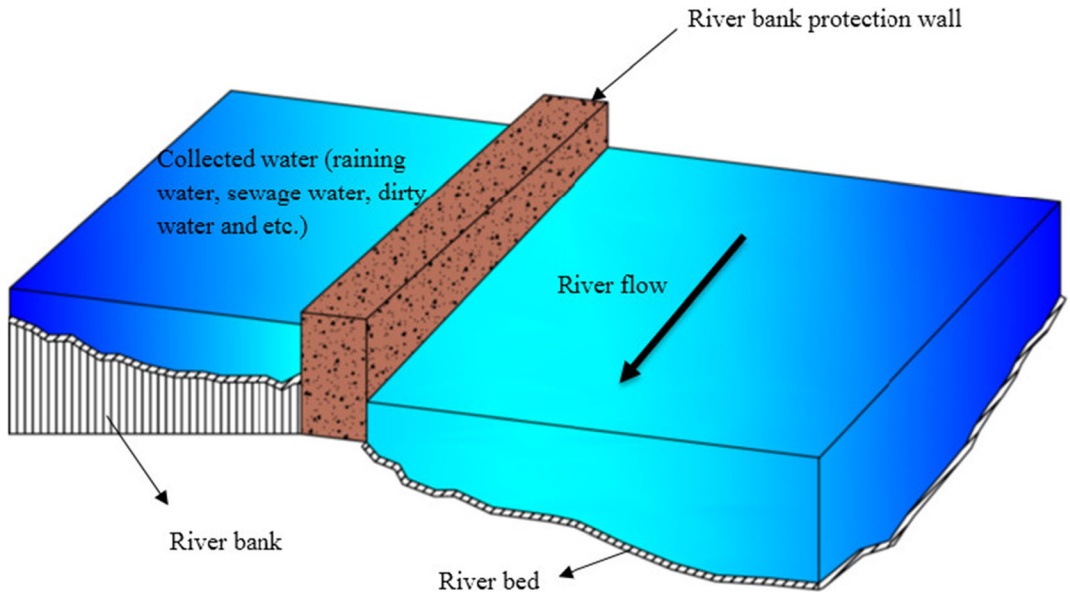

Fig. 14 River bank protection wall as a case for the 3D water seepage analysis

Based on Eqs. (15) and (24), hydraulic head contours were illustrated in Fig. 13. As seen in this figure, the piecewise rectangular distribution of the hydraulic head on the right boundary creates a wrinkle shape in the *h* contours.

Analytical solution for 3D water seepage

Seepage analysis in the river bank (Javdanian and Jafarian 2018) protection walls is an example of the 3D water seepage (Fig. 14). As shown in Fig. 14, on the left side and upstream of the wall is collected water that can be

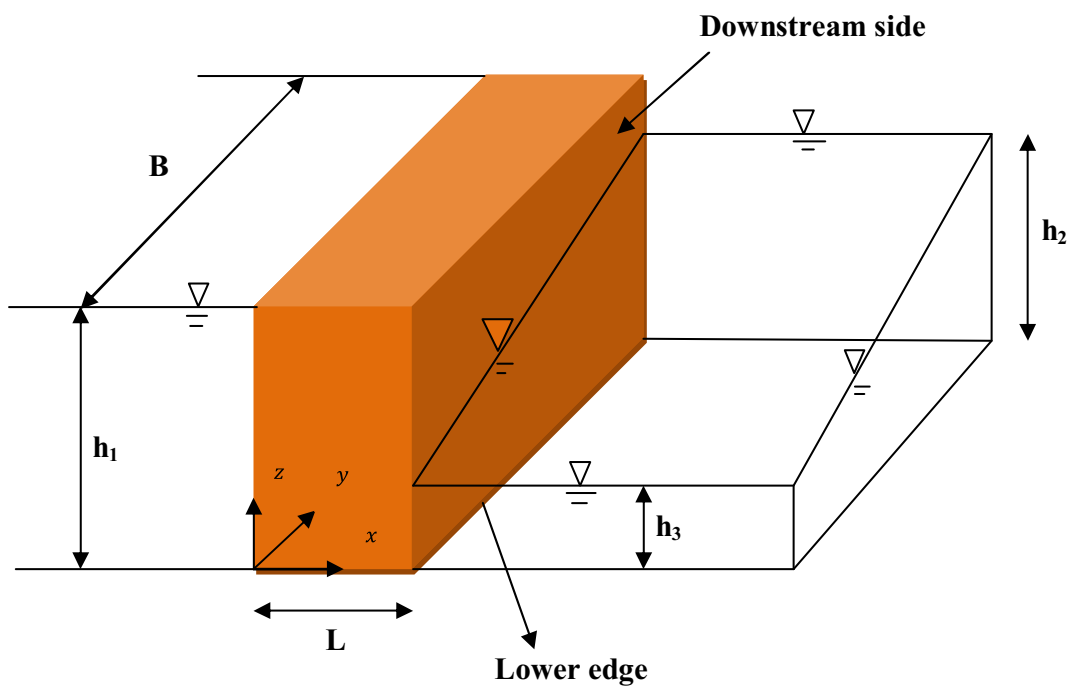

Fig. 15 Solution domain for 3D water seepage analysis with a linear distribution of the hydraulic head at downstream

accumulated because of raining water, sewage water, dirty water, and so forth. The collected water creates a constant hydraulic head at the upstream of the wall. The river has a natural flow on the downstream of the wall. As shown in Fig. 14, the river flow due to the hydraulic gradient creates a linear hydraulic head on the downstream of the wall. Therefore, a constant hydraulic head at the upstream and a linear distribution of the hydraulic head at the downstream of the dam (Fig. 15) were applied. Due to the 3D domain and high hydraulic gradient at the downstream of the dam, there are both vertical and horizontal seepage. As a result, the Dupuit assumptions are not suitable for this case. The governing equation for 3D steady-state water seepage in the isotropic homogeneous dam without Dupuit assumptions is as follows (see Eqs. 1 and 2):

$$\frac{\partial^2 h^2}{\partial x^2}+\frac{\partial^2 h^2}{\partial y^2}+\frac{\partial^2 h^2}{\partial z^2}=0 \tag{27}$$

where h is the hydraulic head (*1/L*). In this case, the no-flow boundary condition is applied to three sides of the dam. Boundary conditions for this case are mathematically expressed as:

$$\frac{\partial h}{\partial z}(x,y,0)=0 \quad h(x,y,h_1)=0 \tag{28-a}$$

$$\frac{\partial h}{\partial y}(x,0,z)=0 \qquad \frac{\partial h}{\partial y}(x,B,z)=0 \tag{28-b}$$

$$h(0,y,z)=h_1 \tag{28-c}$$

$$h(L,y,z)=\left[U(z)-U\left(z-\left(\frac{h_2-h_3}{B}y+h_3\right)\right)\right]\times\left[\frac{h_2-h_3}{B}y+h_3\right] \tag{28-d}$$

where U is the unit step function. Also, h_1, h_2, and h_3 were shown in Fig. 15. The downstream boundary condition for all points below the water table has a linear distribution of the hydraulic head, and for all points above the water table provides zero hydraulic head. Also, this boundary condition provides a constant hydraulic head value for all points located on any vertical line that is perpendicular to the lower edge of the dam at the downstream side.

To find an analytical solution for Eq. (27) with the aforementioned boundary conditions, the variable change as $h^2(x,y,z)=w(x,y,z)$ is used, and then the PDE and the boundary conditions for $w(x,y,z)$ is written as:

$$\frac{\partial^2 w}{\partial x^2}+\frac{\partial^2 w}{\partial y^2}+\frac{\partial^2 w}{\partial z^2}=0 \tag{29}$$

$$\frac{\partial w}{\partial z}(x,y,0)=0 \quad w(x,y,h_1)=0 \tag{30-a}$$

$$\frac{\partial w}{\partial y}(x,0,z)=0 \qquad \frac{\partial w}{\partial y}(x,B,z)=0 \tag{30-b}$$

$$w(0,y,z)={h_1}^2 \tag{30-c}$$

$$w(L,y,z)=\left(\left[U(z)-U\left(z-\left(\frac{h_2-h_3}{B}y+h_3\right)\right)\right]\times\left[\frac{h_2-h_3}{B}y+h_3\right]\right)^2 \tag{30-d}$$

Using separation of variables for $w(x,y,z)$:

$$w(x,y,z)=X(x)\,Y(y)\,Z(z) \tag{31}$$

Substituting Eq. (31) into Eq. (29) gives:

$$\frac{Z''}{Z}=-\left(\frac{X''}{X}+\frac{Y''}{Y}\right)=\mu \tag{32}$$

If $\mu\geq 0$, a trivial solution for *Z (z)* in Eq. (32) would be obtained. If $\mu<0$, assuming $\mu=-\lambda^2$, $\lambda>0$, then by using the boundary conditions of Eq. (30-a), *Z(z)* in Eq. (32) is written as:

$$Z_n=B_2\cos(\lambda z), \quad \lambda=\frac{(2n-1)\,\pi}{2h_1}, \quad n=1,2,3,\ldots,\infty \tag{33}$$

where B_2 is a constant.

Substituting $-\lambda^2$ into Eq. (32) for $\frac{Z'}{Z}$ yields:

$$\frac{Y''}{Y}=\lambda^2-\frac{X''}{X}=\rho \tag{34}$$

where ρ is an arbitrary constant.

If $\rho=0$ and $\rho<0$, say $\rho=-\beta^2$ and $\beta>0$, then by considering the boundary conditions of Eq. (30-b), *Y(y)* in Eq. (34) has two answer as follows:

$$Y_1 = D \tag{35}$$

$$Y_n = B_3\cos(\beta y), \quad \beta = \frac{m.\pi}{B} \quad , \quad m = 1, 2, 3, \ldots, \infty \tag{36}$$

where D and B_3 are constants. For $\rho > 0$, a trivial solution is obtained for $Y(y)$. Substituting $\rho = 0$ and $\rho = -\beta^2$ in Eq. (34) for $\frac{Y''}{Y}$, two equations are obtained:

$$\lambda^2 - \frac{X''}{X} = 0 \tag{37 - a}$$

$$\lambda^2 - \frac{X''}{X} = -\beta^2 \tag{37 - b}$$

The solution of Eq. (37-a) and Eq. (37-b) gives:

$$X_n = A_5\cosh(\lambda x) + A_6\sinh(\lambda x) \tag{38 - a}$$

$$X_{nm} = A_4\cosh(\tau x) + B_4\sinh(\tau x), \quad \tau = \sqrt{(\beta^2 + \lambda^2)} \tag{38 - b}$$

where A_4, A_5, A_6, and B_4 are constants.

By substituting Eqs. (33), (35), and (38-a) into Eq. (31), the first answer for $w(x, y, z)$ yields:

$$w_1(x, y, z) = X_n(x)Y_1(y)Z_n(z) = \sum_{n=1}^{\infty} \left[A_5{}^*\cosh(\lambda x) + A_6{}^*\sinh(\lambda x)\right]\cos(\lambda z) \tag{39}$$

where $A_5{}^*$ is $A_5\, D\, B_2$ and $A_6{}^*$is $A_6\, D\, B_2$.

By substituting Eqs. (33), (36), and (38-b) into Eq. (31), the second answer for $w(x, y, z)$ is written as:

$$w_2(x, y, z) = X_{nm}(x)Y_n(y)Z_n(z) = \sum_{n=1}^{\infty}\sum_{m=1}^{\infty} \left(A_4{}^*\cosh(\tau x) + \mathrm{B}_4^*\sinh(\tau x)\right)\cos(\beta y)\cos(\lambda z) \tag{40}$$

where $A_4{}^*$ is $A_4B_2B_3$ and $\mathrm{B}_4^*$is $B_4B_2B_3$.

Finally, the overall answer for $w(x, y, z)$ is the combination of Eq. (39) and Eq. (40):

$$w(x, y, z) = w_1(x, y, z) + w_2(x, y, z) = \sum_{n=1}^{\infty}\sum_{m=1}^{\infty} \left(A_4{}^*\cosh(\tau x) + \mathrm{B}_4^*\sinh(\tau x)\right)\cos(\beta y)\cos(\lambda z) + \sum_{n=1}^{\infty} \left[A_5{}^*\cosh(\lambda x) + A_6{}^*\sinh(\lambda x)\right]\cos(\lambda z) \tag{41}$$

Substituting the boundary condition of Eqs. (30-c) and (30-d) into Eq. (41) and using Fourier series properties gives:

$$A_4{}^* = \frac{4}{h_1\, B}\int_0^B\int_0^{h_1} h_1^2\cos(\beta y)\cos(\lambda z)\; dz\, dy = 0 \tag{42 - a}$$

$$A_5{}^* = \frac{2}{h_1\, B}\int_0^B\int_0^{h_1} h_1^2\cos(\lambda z)\; dz\, dy = \frac{4h_1^2(-1)^{n+1}}{(2n-1)\pi} \tag{42 - b}$$

$$B_4{}^* = \frac{1}{\sinh(\tau L)} * \frac{4}{h_1\, B}\int_0^B\int_0^{h_1} \left(\left[U(z) - U\left(z - \left(\frac{h_2 - h_3}{B}y + h_3\right)\right)\right] \times \left[\frac{h_2 - h_3}{B}y + h_3\right]\right)^2 \cos(\beta y)\cos(\lambda z)\; dz\, dy \tag{42 - c}$$

$$A_6{}^* = \frac{\frac{2}{h_1\, B}\int_0^B\int_0^{h_1} \left(\left[U(z) - U\left(z - \left(\frac{h_2 - h_3}{B}y + h_3\right)\right)\right] \times \left[\frac{h_2 - h_3}{B}y + h_3\right]\right)^2 \cos(\lambda z)\; dz\, dy - A_5{}^*\cosh(\lambda L)}{\sinh(\lambda L)} \tag{42 - d}$$

Table 3 Hydraulic head values resulted from analytical approach (for different summation truncations) and FDM for 3D water seepage at the vertical section $y = 250$ cm

x (cm)	z (cm)	$h_{analytical}$				h_{FDM}	RE (%)
		$n = m =$ 1~5	$n = m =$ 1~10	$n = m =$ 1~15	$n = m =$ 1~20	$\Delta x = \Delta y = \Delta z = 10$ cm	
30	100	260.92	261.58	262.05	262.05	265.34	1.25
50	150	223.14	223.81	224.37	224.37	227.02	1.18
60	250	159.48	160.02	160.69	160.69	163.21	1.56
80	200	131.56	132.21	132.83	132.83	134.62	1.34
90	250	76.31	77.14	77.73	77.73	79.01	1.64
20	150	270.68	271.23	271.84	271.84	274.35	0.92
10	270	263.09	263.76	264.20	264.20	267.41	1.21
40	180	233.25	233.87	234.47	234.47	237.22	1.17
50	250	182.08	182.71	183.20	183.20	186.31	1.69
90	150	127.33	127.83	128.37	128.37	130.85	1.93

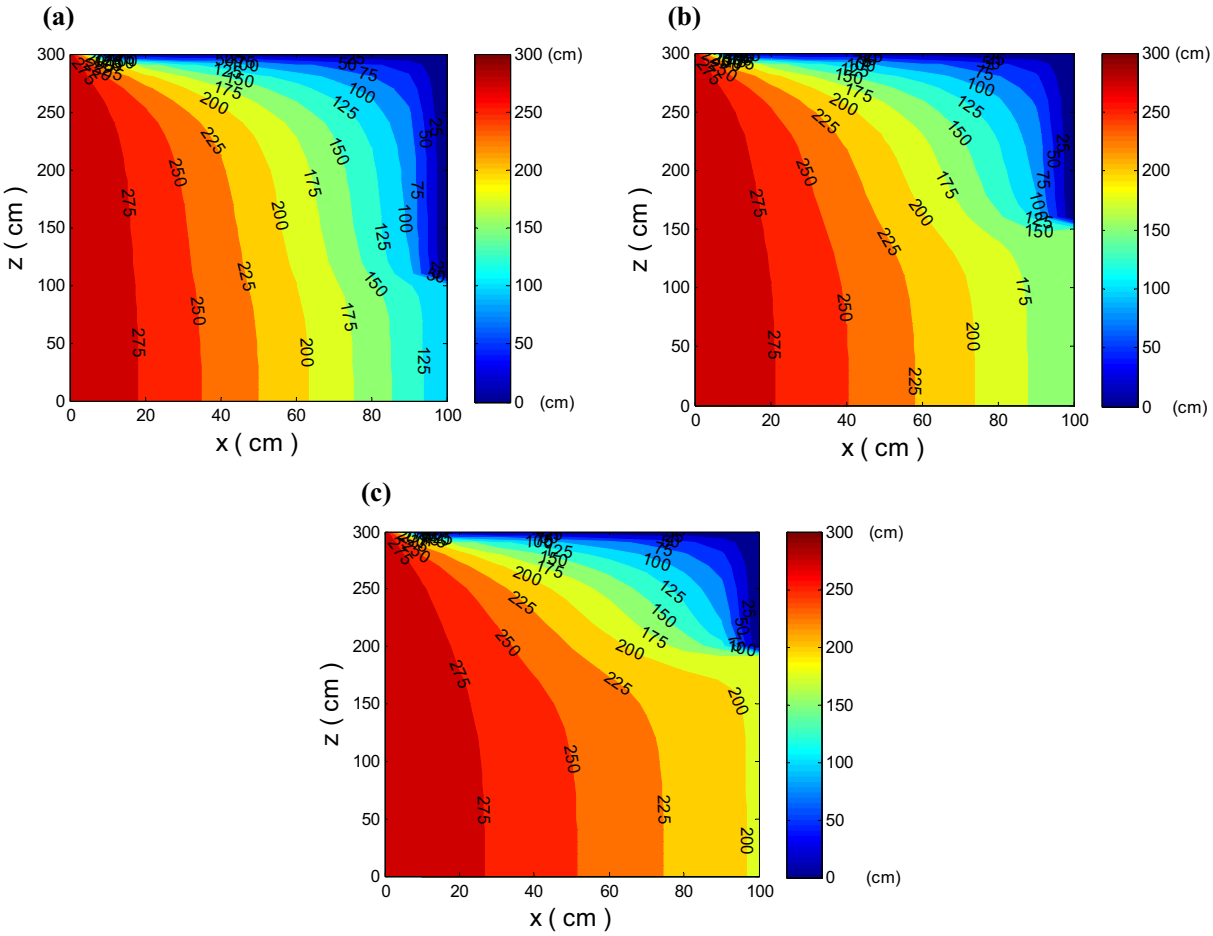

Fig. 16 Hydraulic head contours for 3D water seepage on the vertical sections at: **a** $y = 20$ cm, **b** $y = 250$ cm, **c** $y = 480$ cm

Some of the terms in the answer of the integral Eq. (42-c) with $h_1 = 300$ cm, $h_2 = 200$ cm, $h_3 = 100$ cm, and $B = 500$ cm are as follows:

$$\int_0^{500}\int_0^{300}\left(\left[U(z)-U\left(z-\left(\frac{200-100}{500}y+100\right)\right)\right]\times\left[\frac{200-100}{500}y+100\right]\right)^2\cos\left(\frac{m\pi}{500}y\right)\cos\left(\frac{(2n-1)\pi}{2*300}z\right) \quad (43)$$

$$dz\,dy = 9*10^9*\Big(4(-1)^{1+m}\cos\left(\frac{2}{3}\pi n\right)\pi^2 + 24(-1)^{1+m}\sin\left(\frac{2}{3}\pi n\right)\pi + 432(-1)^{1+m}n\cos\left(\frac{2}{3}\pi n\right)$$

$$+ 576(-1)^{1+m}n^3\cos\left(\frac{2}{3}\pi n\right) + 768(-1)^{1+m}n^3\cos\left(\frac{2}{3}\pi n\right)\sqrt{3}\pi + 320(-1)^{1+m}n^4\sin\left(\frac{2}{3}\pi n\right)\sqrt{3}\pi^2$$

$$+ 192(-1)^{1+m}n\cos\left(\frac{2}{3}\pi n\right)\sqrt{3}\pi + 2304(-1)^{1+m}n^3\pi^2m^2\cos\left(\frac{2}{3}\pi n\right) + 1728(-1)^{1+m}\mathrm{n}\pi^2m^2\cos\left(\frac{2}{3}\pi n\right)$$

$$+ 5184(-1)^{1+m}\pi^2m^4\sin\left(\frac{2}{3}\pi n\right)\sqrt{3} + \ldots\Big)$$

$$/\left(\pi^4\left(1 + 448n^6 - 672n^5 + 560n^4 - 46656m^6 - 280n^3 + 3888m^4 + 84n^2 - 108m^2 + 3456n^5m^2 + \ldots\right)\right)$$

Also, some of the terms in the answer of the integral Eq. (42-d) with $h_1 = 300$ cm, $h_2 = 200$ cm, $h_3 = 100$ cm, and $B = 500$ cm are written as:

$$\int_0^{500}\int_0^{300}\left(\left[U(z)-U\left(z-\left(\frac{200-100}{500}y+100\right)\right)\right]\times\left[\frac{200-100}{500}y+100\right]\right)^2\cos\left(\frac{(2n-1)\pi}{2*300}z\right) \quad (44)$$

$$dz\,dy = \frac{-18*10^9}{(2n-1)^4\pi^4}\times\Big(-72\cos\left(\frac{1}{3}(2n-1)\pi\right) + 72\cos\left(\frac{1}{6}(2n-1)\pi\right) + 4\cos\left(\frac{1}{3}(2n-1)\pi\right)\pi^2$$

$$+ 16\cos\left(\frac{1}{3}(2n-1)\pi\right)\pi^2n^2 - 16\cos\left(\frac{1}{3}(2n-1)\pi\right)\pi^2n + 24\pi\sin\left(\frac{1}{3}(2n-1)\pi\right) - 48\pi n\sin\left(\frac{1}{3}(2n-1)\pi\right) + \ldots\Big)$$

Substituting Eq. (41) into $h^2(x,y,z) = w(x,y,z)$ gives:

$$h^2(x,y,z) = \sum_{n=1}^{\infty}\sum_{m=1}^{\infty}\left(A_4{}^*\cosh(\tau x) + B_4^*\sinh(\tau x)\right)\cos(\beta y) \quad (45)$$
$$\cos(\lambda z) + \sum_{n=1}^{\infty}\left[A_5{}^*\cosh(\lambda x) + A_6{}^*\sinh(\lambda x)\right]$$
$$\cos(\lambda z)$$

In order to test convergence of summations in Eq. (45), hydraulic head at a vertical section ($y =$ 250 cm) is calculated by summations truncations with different amounts of n and m (Table 3). Table 3 is presented for the parameters $h_1 = 300$ cm, $h_2 = 200$ cm, $h_3 = 100$ cm, $B = 500$ cm, and $L = 100$ cm.

To illustrate application of the derived equations, hydraulic head values from an explicit scheme FDM solution (Eq. 27) is compared to the analytical solution (Eq. 45) for different values of x and z (Table 3, columns 7). The eighth column depicts relative error (*RE*) based on column 6 (incorporating > 400 summation terms) and column 7 (FDM for $\Delta x = \Delta y = \Delta z =$ 10 cm). As presented in Table 3, the values of *RE* are less than 2%.

Based on Eq. (45), hydraulic head contours were depicted in Figs. 16(a-c) at the vertical sections of $y =$ 20, 250, and 480 cm, respectively. As seen in these figures, by increasing the y value, hydraulic head increases in all parts of the vertical sections (x-z plane) of the dam (corresponding to Fig. 15 and Eq. 28-d).

Figure 16 illustrates distribution of the hydraulic head that remains at $h = 300$ cm on the left ($x = 0$) and $h =$ Eq. (28-d) on the right ($x = 100$ cm) boundaries in the vertical sections (x-z plane) of the dam.

Summary and conclusions

Innovative analytical solutions for two- and three-dimensional steady-state water seepage through dams with nonsymmetric boundary conditions were derived using separation variables and Fourier series expansion techniques. The nonsymmetric boundary conditions were considered by different unit step functions on a part and/or parts of the boundary of the dam plane. Six two-dimensional cases were studied, where a constant hydraulic head was applied at the left boundary and various hydraulic head distributions including rectangular, ramp, triangular, trapezoidal, tunnel, and piecewise rectangular distributions were applied at the right boundary of the dam plane. Subsequently, a three-dimensional case was investigated so that a constant hydraulic head was applied at the upstream and a linearly distributed hydraulic head was applied at the downstream of the dam. All the boundary conditions and partial differential equations (PDEs) were satisfied by the derived analytical solutions. Subsequently, the performance of the developed analytical methods was assessed in comparison with numerical modeling. The results illustrate reasonable accuracy of the governing equations to assess seepage through media with nonsymmetric boundary conditions. The developed analytical solutions can be used as a reference result to evaluate accuracy and verify the numerical algorithms with similar nonsymmetric boundary conditions.

Acknowledgements This work has been financially supported by the research deputy of Shahrekord University under grant numbers 97GRN1M1830 and 97GRN1M39422. This support is gratefully acknowledged.

References

Chen, J. T., Hong, H. K., & Chyuan, S. W. (1994). Boundary element analysis and design in seepage problems using dual integral formulation. *Finite Elements in Analysis and Design, 17*, 1–20.

Chesnaux, R. (2016). Closed-form analytical solutions for assessing the consequences of sea-level rise on unconfined sloping island aquifers. *Global and Planetary Change, 139*, 109–115.

El Tani, M., Kamali, A., & Gholami, M. A. (2019). Analytic assessment of the water table drawdown, seepage, and back pressure at Rudbar PSPP. *Rock Mechanics and Rock Engineering, 52*(7), 2227–2243.

Fu, J., & Jin, S. (2009). A study on unsteady seepage flow through dam. *Journal of Hydrodynamics, 21*, 499–504.

Fukuchi, T. (2016). Numerical analyses of steady-state seepage problems using the interpolation finite difference method. *Soils and Foundations, 56*, 608–626.

Fusi, L., Farina, A., & Rosso, F. (2015). Mathematical models for fluids with pressure-dependent viscosity flowing in porous media. *International Journal of Engineering Science, 87*, 110–118.

Javdanian, H. (2019). Predicting seismic slope displacements of embankment dams using fuzzy systems. *Journal of Dam and Hydroelectric Powerplant, 5*(19), 25–35.

Javdanian, H., & Jafarian, Y. (2018). Dynamic shear stiffness and damping ratio of marine calcareous and siliceous sands. *Geo-Marine Letters, 38*(4), 315-322.

Javdanian, H., & Lee, S. (2019). Evaluating unconfined compressive strength of cohesive soils stabilized with geopolymer: a computational intelligence approach. *Engineering with Computers, 35*(1), 191-199.

Javdanian, H. (2019). Evaluation of soil liquefaction potential using energy approach: experimental and statistical investigation. *Bulletin of Engineering Geology and the Environment, 78*(3), 1697-1708.

Javdanian, H., & Pradhan, B. (2019). Assessment of earthquake-induced slope deformation of earth dams using soft computing techniques. *Landslides, 16*(1), 91–103.

Javdanian, H., Shakarami, L., & Zarif Sanayei, H. R. (2018a). Modeling seismic settlement of earth dams due to earthquake loading. International conference on new findings of civil, architectural and Iran building industry, 11 December, Tehran.

Javdanian, H., Zarif Sanayei, H. R., & Shakarami, L. (2018b). A regression-based approach to predict crest settlement of embankment dams under earthquake shaking. *Scientia Iranica*. https://doi.org/10.24200/sci.2018.50483.1716.

Kacimov, A., & Obnosov, Y. (2012). Analytical solutions for seepage near material boundaries in dam cores: the Davison–Kalinin problems revisited. *Applied Mathematical Modelling, 36*, 1286–1301.

Kacimov, A. R., & Obnosov, Y. V. (2019). Modelling of 2-D seepage from aquifer towards stream via clogged bed: the toth-trefftz legacy conjugated. *Advances in Water Resources, 131*, 103372.

Kazemzadeh-Parsi, M. J., & Daneshmand, F. (2013). Three dimensional smoothed fixed grid finite element method for the solution of unconfined seepage problems. *Finite Elements in Analysis and Design, 64*, 24–35.

Leontiev, A., & Huacasi, W. (2001). Mathematical programming approach for unconfined seepage flow problem. *Engineering Analysis with Boundary Elements, 25*, 49–56.

Li, M., Guo, X., Shi, J., & Zhu, Z. (2017). Seepage and stress analysis of anti-seepage structures constructed with different concrete materials in an RCC gravity dam. *Water Science and Engineering, 8*, 326–334.

Liang, X., & Zhang, Y. K. (2013). Analytic solutions to transient groundwater flow under and time-dependent sources in a heterogeneous aquifer bounded by fluctuating river stage. *Advances in Water Resources, 58*, 1–9.

Mohsenian, A. R., Sedghi-Asl, M., & Rahimi, H. (2019). An analytical solution for confined seepage problem beneath hydraulic structures. *Iranian Journal of Science and Technology, Transactions of Civil Engineering, 43*(2), 361–369.

Nasiri, F., Javdanian, H., & Heidari, A. (2019). Behavior of earth dams due to downsampling-based records. In: 8th International Conference on Seismology and Earthquake Engineering (SEE8), 11 November, Tehran, Iran.

Navas, P., Lopez-Querol, S., Yu, R. C., & Li, B. (2016). B-bar based algorithm applied to meshfree numerical schemes to solve unconfined seepage problems through porous media. *International Journal for Numerical and Analytical Methods in Geomechanics, 40*(6), 962–984.

Nourani, V., Aminfar, M. H., Alami, M. T., Sharghi, E., & Singh, V. P. (2014). Unsteady 2-D seepage simulation using physical analog, case of Sattarkhan embankment dam. *Journal of Hydrology, 519*, 177–189.

Pedroso, D. M. (2015). A solution to transient seepage in unsaturated porous media. *Computer Methods in Applied Mechanics and Engineering, 285*, 791–816.

Rakhshandehroo, G. R., & Pourtouiserkani, A. (2013). Predicting Doroodzan dam hydraulic behavior during rapid drawdown. *Iranian Journal of Science and Technology, Transaction of Civil Engineering, 37*, 301–310.

Rezk, M. A. E. R. M., & Senoon, A. E. A. A. A. (2012). Analytical solution of earth dam with upstream blanket. *Alexandria Engineering Journal, 51*, 45–51.

Serrano, S. E., & Workman, S. R. (1998). Modeling transient stream/aquifer interaction with the non-linear Boussinesq equation and its analytical solution. *Journal of Hydrology, 206*, 245–255.

Shakarami, L., Javdanian, H., Zarif Sanayei, H. R., & Shams, G. (2019). Numerical investigation of seismically induced crest settlement of earth dams. *Modeling Earth Systems and Environment, 5(4)*, 1231–1238.

Tan, X., Wang, X., Khoshnevisan, S., Hou, X., & Zha, F. (2017). Seepage analysis of earth dams considering spatial variability of hydraulic parameters. *Engineering Geology, 228*, 260–269.

Teloglou, I. S., & Bansal, R. K. (2012). Transient solution for stream–unconfined aquifer interaction due to time varying stream head and in the presence of leakage. *Journal of Hydrology, 428*, 68–79.

Wei, B., Gu, M., Li, H., Xiong, W., & Xu, Z. (2018). Modeling method for predicting seepage of RCC dams considering time-varying and lag effect. *Structural Control and Health Monitoring, 25*(2), 1–14.

Yuan, S., & Zhong, H. (2016). Three dimensional analysis of unconfined seepage in earth dams by the weak form quadrature element method. *Journal of Hydrology, 533*, 403–411.

Zarif Sanayei, H. R., Talebbeydokhti, N., & Moradkhani, H. (2015). 3D estimation of metal elements in sediments of the Caspian Sea with moving least square and radial basis function interpolation methods. *Scientia Iranica, Transaction A: Civil Engineering, 22*(5), 1661–1673.

Zarif Sanayei, H. R., Talebbeydokhti, N., & Rakhshandehroo, G. R. (2019). Analytical solutions for water infiltration into unsaturated–semi-saturated soils under different water content distributions on the top boundary. *Iranian Journal of Science and Technology, Transactions of Civil Engineering*, 43(4), 747–760.

Zhang, W., Dai, B., Liu, Z., & Zhou, C. (2017). Unconfined seepage analysis using moving kriging mesh-free method with Monte Carlo integration. *Transport in Porous Media, 116*(1), 163–180.